Singular energy component for identification of initial delamination in CFRP laminates through piezoelectric actuation and non-contact measurement

Wei Xu[1,2,3], Zhongqing Su[2], Jingqiang Liu[4*],

Maosen Cao[1,3*], Wiesław Ostachowicz[5]

[1] Jiangxi Provincial Key Laboratory of Environmental Geotechnical Engineering and Disaster Control, Jiangxi University of Science and Technology, Ganzhou 341000, China

[2] Department of Mechanical Engineering, The Hong Kong Polytechnic University, Hung Hom, Kowloon, Hong Kong, China

[3] Department of Engineering Mechanics, Hohai University, Nanjing 210098, China

[4] College of Water Conservancy and Civil Engineering, Shandong Agricultural University, Taian 271018, China

[5] Institute of Fluid-Flow Machinery, Polish Academy of Sciences, Gdańsk 80-231, Poland

---

[*]Corresponding authors.
E-mail addresses: weixu@polyu.edu.hk, wxu@hhu.edu.cn (W. Xu), zhongqing.su@polyu.edu.hk (Z. Su), jqliu@sdau.edu.cn (J. Liu), cmszhy@hhu.edu.cn (M. Cao), wieslaw.ostachowicz@imp.gda.pl (W. Ostachowicz)

Abstract: Delamination is typically barely visible impact damage (BVID) in carbon fiber reinforced polymer (CFRP) laminates. It is important to identify initial delamination in the early stage. The concept of 2D multi-resolution modal Teager-Kaiser energy (MRM-TKE^{2D}) was recently proposed to reveal delamination-caused singularity in a mode shape for delamination identification with high robustness against environmental noise. However, inadequate sensitivity impairs its capability to identify initial delamination. A damage indicator needs to be further formulated to characterize the presence and location of initial delamination. To address this problem, a scheme of decomposing MRM-TKE^{2D} into components is proposed for identification of initial delamination. Among the energy components of the MRM-TKE^{2D} for a CFRP laminate with an initial delamination, a singular energy component is dominated by the delamination and can be determined by its spectral entropy. In the singular energy component, energy converges into the delamination region to form a singular peak and almost vanishes in other places, from which the presence and location of the initial delamination can be characterized by the singular peak. This method is numerically verified on CFRP laminates with initial delamination. Its applicability is experimentally validated by identifying an initial delamination in a CFRP laminate, the mode shapes of which are acquired by piezoelectric actuation using a lead-zirconate-titanate (PZT) actuator and non-contact measurement using a scanning laser vibrometer (SLV). Numerical and experimental results show that singular energy components are capable of identifying initial delamination under noisy environments.

Keywords: CFRP laminate; Initial delamination; 2D multi-resolution modal Teager-Kaiser energy; Singular energy component; Piezoelectric actuation; Non-contact measurement

1. Introduction

Delamination is typically barely visible impact damage (BVID) in carbon fiber reinforced polymer (CFRP) laminates. It is important to identify delamination in the early stage before initial delamination accumulates and develops to weaken the integrity and stiffness of the laminates [1, 2].

Delamination detection using nondestructive testing techniques such as X-ray [3], C-scan [4], ultrasonic imaging [5], strain [6-10], eddy current [11, 12], electrical potential [13], thermography [14-17], shearography [18], guided wave [19-23], and vibro-acoustics [24-28] methods have been widely developed in the past decades. Their common limitation is that the approximate delamination region needs to be known *a priori* [29]. In recent years, delamination identification methods relying on mode shapes have attracted increasing attention because global spatial information of the laminate is contained within mode shapes. Delamination can cause local changes in the derivatives of mode shapes, whereby its presence and location can be characterized. Representative studies are as follows. Qiao et al. [30] evaluated and compared three typical mode-shape-based algorithms (i.e., the simplified gapped smoothing method (GSM), the generalized fractal dimension (GFD), and the strain energy method (SEM)) for identification of delamination in composite laminated plates. Araújo dos Santos et al. [31] used TV holography to measure mode shapes of a composite laminate subject to acoustic excitation. Modal curvature differences of laminates under structurally intact and damaged statuses could be used to identify impact-caused delamination. Pérez et al. [32] used natural frequencies and modal curvatures of intact and damaged composite laminates to formulate a curvature damage factor, by which the location of impact-caused delamination could be determined. Cao et al. [33] proposed a new concept of multiscale shear-strain gradient for detecting delamination in composite

laminates. The capability of the proposed concept was validated on a glass fiber reinforced polymer (GFRP) laminate bearing a heat-caused delamination. Xu et al. [34] formulated the complex-wavelet curvature mode shape for identification of delamination in composite laminates. Superior to the conventional curvature mode shape, it features higher sensitivity to damage and robustness to noise interference. Chen et al. [35] developed a continuously scanning laser Doppler vibrometer (CSLDV) to measure vibration shapes of a laminated composite plate with a delamination. Local anomalies in vibration shapes could be used to identify the delamination.

However, initial delamination can barely cause evident changes in mode shapes or their derivatives. With this concern, Solodov et al. [36] selected the specific mode shape at the local defect resonance where the vibration amplitude in the delamination region could be strongly enhanced, by which means the initial delamination could be clearly detected and located. For ordinary mode shapes, Xu et al. [37] recently formulated a concept of multi-resolution 2D modal Teager-Kaiser energy (MRM-TKE^{2D}), which is the point-wise energy of a mode shape and is capable of identifying delamination under noisy environments. However, inadequate sensitivity impairs its capability to identify initial delamination. A damage indicator (DI) needs to be further formulated to characterize the presence and location of initial delamination.

Addressing the inadequate sensitivity of the MRM-TKE^{2D} to initial delamination, a scheme of decomposing the MRM-TKE^{2D} into components is proposed for identification of initial delamination. In a CFRP laminate with an initial delamination, its MRM-TKE^{2D} can be decomposed into components by the singular value decomposition (SVD). Among these components, a singular energy component can be discovered dominated by the delamination, in which energy converges into the delamination region to form a singular peak and almost vanishes in other places.

Thereby, the presence and location of the initial delamination can be characterized by the singular peak.

The rest of the paper is organized as follows. Section 2 formulates the concept of a singular energy component for identifying delamination. Section 3 numerically verifies the concept of the singular energy component for the identification of initial delamination in CFRP laminates. Section 4 experimentally validates the proposed method on a CFRP laminate with an initial delamination. The delaminated CFRP laminate is excited by high-frequency harmonic waves using a lead-zirconate-titanate (PZT) piezoelectric actuator, and its high resolution mode shapes are acquired through non-contact measurement using a scanning laser vibrometer (SLV). Although an early PZT-SLV system has been used for identification of delamination in composite laminates [30], it lacks capability to identify initial delamination due to its low excitation frequency and spatial sampling density. In this study, the PZT-SLV system is enhanced. High-frequency harmonic waves at kilohertz are generated by a PZT piezoelectric actuator to excite a composite laminate, whereby its high-order modes can be achieved; synchronously, corresponding high-order mode shapes are measured with millimeter-level high resolution by a non-contact SLV to capture details of the initial delamination. Section 5 presents concluding remarks of this paper.

2. Singular energy component for delamination identification

2.1. Delamination-caused change in mode shapes

The vibration of a M-ply cross-ply laminate made of 0/90° orientations can be expressed as

$$D_{11}\frac{\partial^4 w}{\partial x^4} + 2(D_{12} + 2D_{66})\frac{\partial^4 w}{\partial x^2 \partial y^2} + D_{22}\frac{\partial^4 w}{\partial y^4} + \bar{\rho}\frac{\partial^2 w}{\partial t^2} = q, \tag{1}$$

where $w(x,y,t)$ is the out-of-plane displacement in the middle surface with time t

and coordinates x and y, $q(x,y,t)$ is the transverse load on the laminate,

$D_{uv} = \dfrac{1}{3}\sum\limits_{d=1}^{M}\overline{Q}_{uv}^{(d)}(z_d^3 - z_{d-1}^3)$ with $u = 1, 2, 6$ and $v = 1, 2, 6$ are stiffness coefficients

ply-wise integrated over the thickness with z_d being the distance from the middle

surface to the surface of the dth ply having the furthest z-coordinate,

$\overline{\rho} = \sum\limits_{d=1}^{M}\rho^{(d)}(z_d - z_{d-1})$ is the average mass density of the plate per unit area of the

midsurface with $\rho^{(d)}$ the density of the dth lamina per unit volume, and the $\overline{Q}_{uv}^{(d)}$ are

the material constants for the dth ply, as can be found in Ref. [38].

For a delaminated composite laminate whose delamination region is represented

by Ω, reduction in stiffness will be caused by the delamination [39]. Stiffness

coefficients $D_{uv}(x, y)$ of the laminate can be written as

$$D_{uv}(x, y) = \begin{cases} D_{uv}^{I} & x, y \notin \Omega \\ D_{uv}^{D} & x, y \in \Omega \end{cases}, \tag{2}$$

where D_{uv}^{I} and D_{uv}^{D} represent the stiffness coefficients under the structurally intact

and delaminated statuses, respectively.

Substituting equation (2) into equation (1) and rearranging equation (1) [40], we

have

$$D_{11}^{I}\frac{\partial^4 w}{\partial x^4} + 2(D_{12}^{I} + 2D_{66}^{I})\frac{\partial^4 w}{\partial x^2 \partial y^2} + D_{22}^{I}\frac{\partial^4 w}{\partial y^4} + \overline{\rho}\frac{\partial^2 w}{\partial t^2} = q + f_{DF}, \tag{3}$$

where f_{DF} is defined as the delamination-caused force (DF):

$$f_{DF} = \begin{cases} 0 & x, y \notin \Omega \\ \Delta \mathbf{D} \cdot \mathbf{\Theta}(w) & x, y \in \Omega \end{cases}, \tag{4}$$

with $\Delta\mathbf{D} = (D_{11}^I - D_{11}^D, (D_{12}^I + 2D_{66}^I) - (D_{12}^D + 2D_{66}^D), D_{22}^I - D_{22}^D)$ denoting the stiffness change vector, and $\mathbf{\Theta}(w) = (\dfrac{\partial^4 w}{\partial x^4}, \dfrac{2\partial^4 w}{\partial x^2 \partial y^2}, \dfrac{\partial^4 w}{\partial y^4})$.

Regarding the elements of the laminate bearing no transverse load, i.e., $q=0$, equation (3) becomes

$$D_{11}^I \frac{\partial^4 w}{\partial x^4} + 2(D_{12}^I + 2D_{66}^I)\frac{\partial^4 w}{\partial x^2 \partial y^2} + D_{22}^I \frac{\partial^4 w}{\partial y^4} + \bar{\rho}\frac{\partial^2 w}{\partial t^2} = f_{DF}. \tag{5}$$

$w(x,y,t)$ can be further written as $W(x,y)\sin(\omega t)$ when W represents a mode shape associated with the corresponding natural frequency ω

The DF applied on the delamination region is generated by the change in the stiffness coefficients induced by the delamination. Conversely, the DF will cause singularity of mode shape in the delamination region. However, with an initial delamination of only several square centimeters, such singularity can barely be observed, even in high-order mode shapes.

2.2. Multi-resolution 2D modal Teager-Kaiser energy

The MRM-TKE^{2D}, denoted as E_N, was recently proposed to reveal delamination-caused singularities in mode shapes of CFRP laminates, with high robustness against environmental noise [37]. The concept of MRM-TKE^{2D} can be formulated by two steps. In the first step, a measured mode shape $W[x,y]$ is decomposed by the discrete wavelet transform (DWT) [41]. By dilating and translating a mother wavelet function $\psi(x,y)$ at level j, we obtain the wavelet function:

$$\psi_{j,k,l}(x,y) = 2^{-j}\psi(2^{-j}x - k, 2^{-j}y - l); \qquad j,k,l \in \Box. \tag{6}$$

Similarly, the scale function $\phi_{j,k,l}(x,y)$ can be dilated and translated from $\phi(x,y)$:

$$\phi_{j,k,l}(x,y) = 2^{-j}\phi(2^{-j}x - k, 2^{-j}y - l); \qquad j,k,l \in \Box. \tag{7}$$

Spanned by $\psi_{j,k,l}(x,y)$, $W[x,y]$ can be decomposed the into the first to the Nth levels:

$$W[x,y] = A_N[x,y] + \sum_{j=1}^{N} D_j[x,y],$$ (8)

where A_N is the approximation at the Nth level, and D_j is the detail at the jth level. Details of the DWT can be found in Ref. [41]. At a satisficing level N, by discarding details D_j ($j = 1,...,N$) that contain noise components and retaining approximation A_N that contains delamination features, the measured mode shape $W[x,y]$ can be de-noised.

In the second step, the 2D Teager-Kaiser (TKE^{2D}) operator [42, 43], denoted as Ψ^{2D}, is applied on the A_N, whereby the MRM-TKE^{2D} is formulated:

$$\begin{aligned} E_N[x,y] &= \Psi^{2D}(A_N[x,y])) \\ &= 2A_N[x,y]^2 - A_N[x-1,y]A_N[x+1,y] - A_N[x,y-1]A_N[x,y+1]. \end{aligned}$$ (9)

The MRM-TKE^{2D} is the point-wise energy of a mode shape and is robust to noise interference. In the MRM-TKE^{2D}, the delamination can cause local change in the delamination region, from which delamination features can be revealed for identification.

2.3. Singular energy component dominated by delamination

For initial delamination, however, delamination-caused changes in the MRM-TKE^{2D} are usually slight. Such slight changes can be obscured by the fluctuant global trends of the MRM-TKE^{2D} and become ambiguous for delamination identification [37]. With this concern, a scheme of decomposing the MRM-TKE^{2D} is proposed in this study, by which means delamination features can be extracted from the delamination-dominated component. As matrices of the MRM-TKE^{2D} are not necessarily square, the SVD instead of the eigendecomposition is used for matrix decomposition [44]:

$$E_N[x, y] = \sum_{r=1}^{R} C_N^r[x, y] = \mathbf{U}\mathbf{\Sigma}\mathbf{V}^{\mathrm{T}}, \tag{10}$$

$$C_N^r[x, y] = \sigma_r \mathbf{u}_r \mathbf{v}_r^{\mathrm{T}}, \tag{11}$$

where E_N represented by an $m \times n$ matrix with the rank of R is decomposed into components $C_N^r[x, y]$ ($r = 1, 2, ..., R$), $\mathbf{U} = \{\mathbf{u}_1, \mathbf{u}_2, ..., \mathbf{u}_m\}$ is an $m \times m$ matrix, $\mathbf{\Sigma}$ is an $m \times n$ matrix with singular values $\sigma_1, \sigma_2, ..., \sigma_R$ in descending order, $\mathbf{V} = \{\mathbf{v}_1, \mathbf{v}_2, ..., \mathbf{v}_n\}$ is an $n \times n$ matrix. For an intact laminate, the first several energy components approximately constitute the global trend of E_N, and subsequent noisy energy components are dominated by residual noise in E_N. However, when the laminate bears a delamination, an energy component dominated by the delamination appears, which is assumed to be distinct from other energy components. In this energy component dominated by the delamination, namely the singular energy component, energy is supposed to converge into the delamination region to form a singular peak and almost vanish in other places, whereby the presence and location of the initial delamination can be characterized by the singular peak.

3. Proof of concept

3.1. Numerical specimen

An eight-layer CFRP symmetric cross-ply laminate made of 0/90º orientations is considered as a specimen, the dimensions of which are 500 mm × 500 mm × 3 mm in the x-, y-, and z-directions, respectively. The boundary conditions for all edges of the laminate are free. The laminate is modeled by the finite element (FE) software ANSYS with eight-node hexahedral elements whose dimensions are 1.25 mm × 1.25 mm × 0.375 mm in the x-, y-, and z-directions, respectively. The elastic modulus in 0º and 90º are E_{11} 92 GPa and E_{22} 8 GPa, respectively; in-plane shear modulus, Poisson's ratio,

and material density are G_{12} 2.9 GPa, ν_{12} 0.33, and ρ 1400 Kgm^{-3}, respectively. An initial delamination is modeled by inserting a small-sized non-thickness interface between interfaces of the second and third plies; on the non-thickness interface of the delamination, the coincident nodes in adjacent but separated elements are distributed. The delamination is centered at x=125 mm and y=375 mm (illustrated in figure 1). Without loss of generality, by introducing the dimensionless coordinates $\zeta = \dfrac{x}{500}$ and $\eta = \dfrac{y}{500}$, the delamination is centered at $\zeta = 0.25$ and $\eta = 0.75$. Scenarios I, II, and III (listed in Table 1) with decreasing delamination areas of 40 mm $\times$ 40 mm, 30 mm $\times$ 30 mm, and 20 mm $\times$ 20 mm respectively are considered for numerical verification.
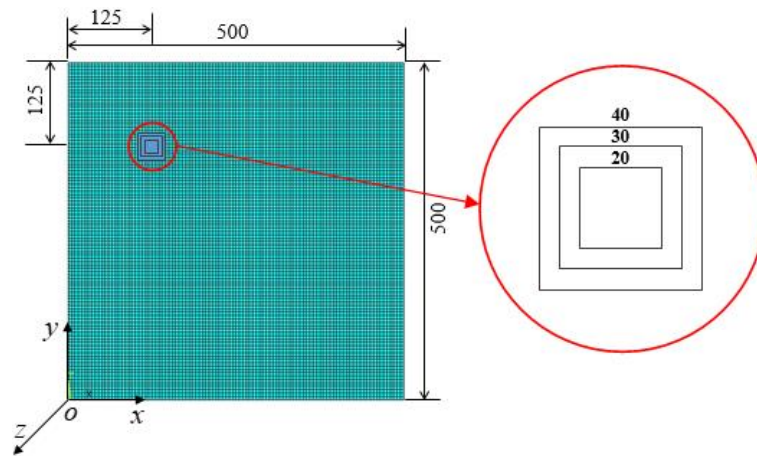
Figure 1. Delaminated CFRP laminate with dimensions in millimeters.

Table 1. Damage Scenarios I-VI

	I	II	III	IV	V	VI
x (mm)	105-145	110-140	115-135	115-135	115-135	115-135
ζ	0.21-0.29	0.22-0.28	0.23-0.27	0.23-0.27	0.23-0.27	0.23-0.27
y (mm)	355-395	360-390	365-385	365-385	365-385	365-385
η	0.71-0.79	0.72-0.78	0.73-0.77	0.73-0.77	0.73-0.77	0.73-0.77
SNR (dB)	80	80	80	70	60	50

3.2. Singular energy component

By modal analysis, the high-order mode shapes in the z-direction are extracted from out-of-plane displacements of 401×401 densely-distributed nodes on the back surface with the interval being 1.25 mm; for generality, each mode shape is of a unit maximum amplitude. To simulate the environmental noise effect on measured mode shapes, white Gaussian noise is added to the noise-free mode shapes to constitute noisy measured mode shapes with signal-to-noise ratio (SNR) 80 dB. Taking Scenario I for illustration, the 21st out-of-plane mode shape at 956.8 Hz is arbitrarily selected, the MRM-TKE^{2D} at the fourth DWT level E_4 can be obtained by equations (8) and (9) and is shown in figure 2, where the delamination causes barely any pronounced features indicative of delamination. As per equations (10) and (11), components decomposed from E_4 are also shown in figure 2. Among these energy components, the first four energy components constitute the global trend of the MRM-TKE^{2D} (weights of C_4^1 and C_4^2 are 78.13% and 9.43%, respectively); the seventh energy component C_4^7 can be found as the singular energy component because it bears a sharply rising singular peak that appears in the delamination region and almost vanishes in other places; subsequent energy components become noisy because they are dominated by residual noise in E_4.
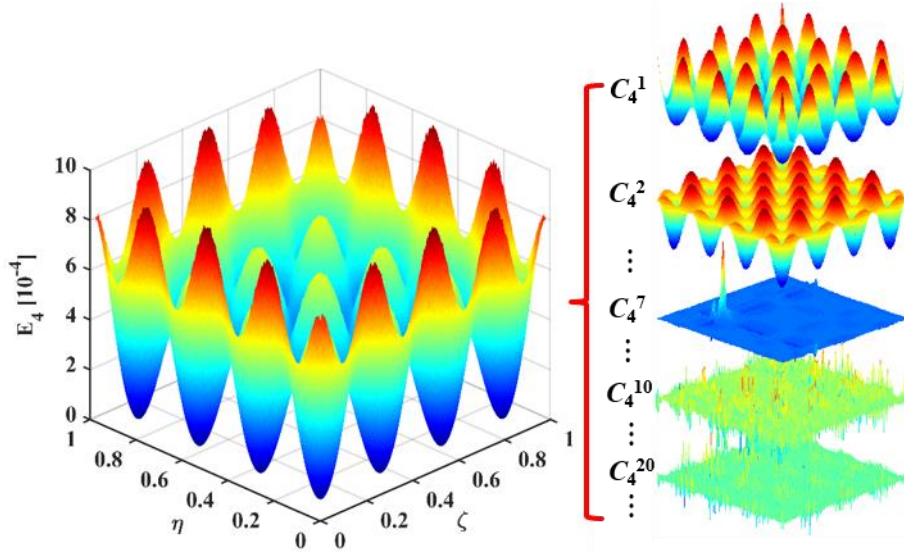
Figure 2. MRM-TKE^{2D} and its components for Scenario I.

However, it is time consuming to inspect energy components one by one to find the singular energy component. To improve efficiency, the spectral entropy [45] of each energy component is calculated to determine the range in which the singular energy component could appear:

$$SE_x^r = -\sum_{g=1} p_{x,g}^r \log_2(p_{x,g}^r),$$ (12)

$$SE_y^r = -\sum_{g=1} p_{y,g}^r \log_2(p_{y,g}^r),$$ (13)

$$SE_N^r = \frac{SE_x^r + SE_y^r}{2},$$ (14)

where $p_{x,g}^r = F_{x,g}^r / \sum_{s=1} F_{x,s}^r$ and $p_{y,g}^r = F_{y,g}^r / \sum_{s=1} F_{y,s}^r$ are the proportions for the gth Fourier counterparts $F_{x,g}^r$ and $F_{y,g}^r$ that are calculated from the middle row and column in matrix $C_N^r[x, y]$ by the fast Fourier transform (FFT) in x- and y-directions, respectively; SE_x^r and SE_y^r are the corresponding spectral entropy whose values are between 0 and 1; the mean value of the SE_x^r and SE_y^r is defined as the spectral

entropy for the rth energy component $C_N^r[x, y]$, denoted as SE_N^r.

As per the definition of the spectral entropy [45], wider distribution of the Fourier counterparts in the frequency spectrum produces higher value of spectral entropy, because more information is included. The spectral entropies of the MRM-TKE^{2D} E_4 for Scenarios I, II, and III are calculated by equations (12) to (14) and shown in figure 3. It can be seen from figure 3 that the spectral entropies can be divided into three statuses indicated by two grey dashed lines, namely the global trend status, the transient status, and the noise status. In the global trend status with r ranging from 1 to 4, the spectral entropies are of low value because MRM-TKE^{2D} components concentrate in a narrow frequency band. In the transient state with r ranging from 5 to 10, values of the spectral entropies increase rapidly because more uncertain information is introduced and is distributed in a wider frequency band. Singular energy components for Scenarios I, II, and III can be found in this status. In the noise status with r exceeding 10, the MRM-TKE^{2D} components are totally contaminated by noise which is evenly distributed in the entire frequency spectrum. Eventually, the spectral entropies approach the upper limit in this status.
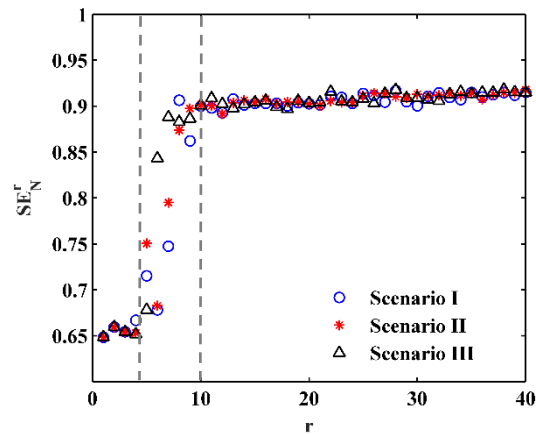
Figure 3. Spectral entropies of MRM-TKE^{2D} components for Scenarios I, II, and III.

3.3. Delamination identification by singular energy component

In transient statuses for Scenarios I, II, and III, their seventh energy components are found to be the corresponding singular energy components, shown in figures 4(a), (c), and (e), with their planforms in figures 4(b), (d), and (f), respectively. It can be seen from figure 4 that the energy in each singular energy component converges into the delamination region to form a singular peak and almost vanishes in other places. In the planforms, those singular peaks clearly characterize the presence and locations of the delaminations: the identified delaminations are centered at $\zeta = 0.25$ and $\eta = 0.75$, spanning about 0.08 (Scenarios I), 0.06 (Scenarios II), and 0.04 (Scenarios III) in both $\zeta -$ and $\eta -$ directions, respectively, which correspond to the actual locations and sizes of the delaminations. It is worth mentioning that a pair of orthogonal ridges of each singular peak propagate in the $\zeta -$ and $\eta -$ directions, because the MRM-TKE^{2D} are totalled in these two directions as shown in equation (9).

Worth to be noted, best frequency of excitation for delamination identification is structure-dependent, and for each structure it needs to be carefully selected after trials to acquire best modes that are sensitive to damage. It is also worth noting that the initial delaminations in Scenarios I, II, and III are too slight to cause the change in the natural frequency (956.8 Hz) of the intact laminate.

(a)   (c)   (e)
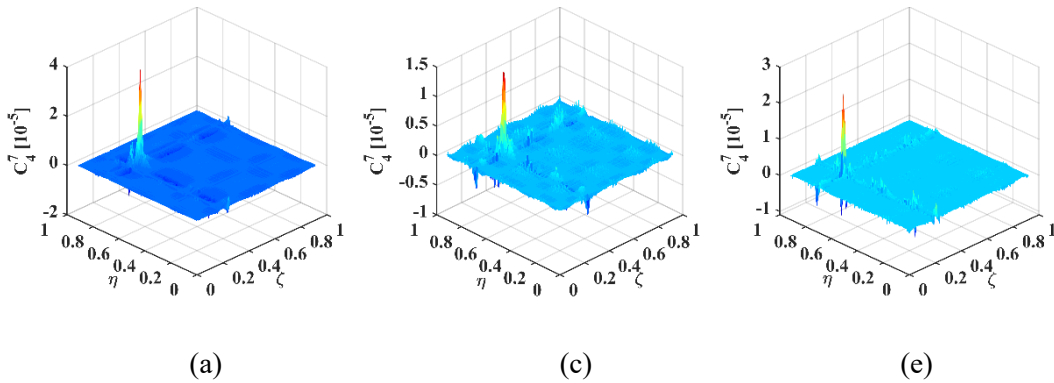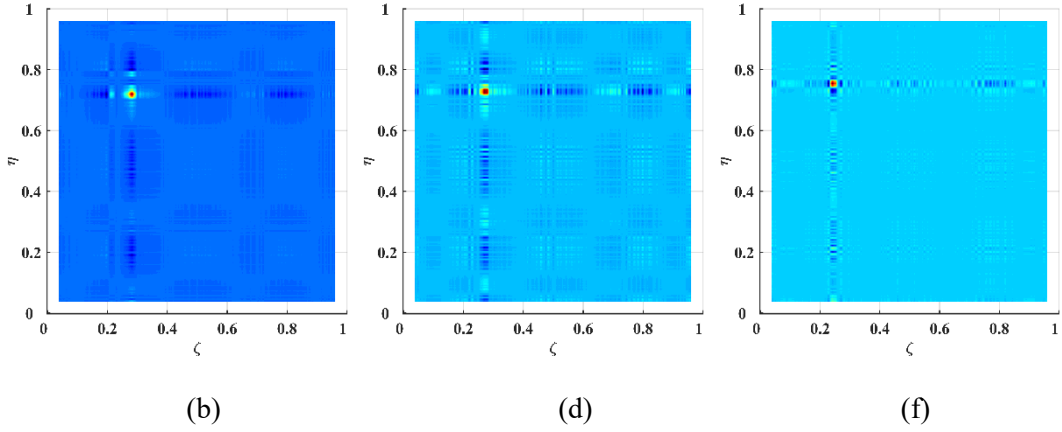
Figure 4. Singular energy components for Scenarios (a) I, (c) II, and (e) III, and their

planforms (b) I, (d) II, and (f) III.

3.4. Robustness against noise interference

To verify the robustness of the singular energy component against environmental noise interference, noisier levels with lower SNRs are considered. Scenario III with the smallest delamination size 20 mm × 20 mm is associated with decreasing SNRs 70 dB, 60 dB, and 50 dB, denoted as Scenarios IV, V, and VI, respectively (listed in Table 1). It can be seen from Scenario IV with SNR 70 dB (shown in figures 5(a) and (b)) that the singular peak clearly designates the presence and location of the delamination as the results of Scenario III (figures 4(e) and (f)). When the noise intensity is increased to SNR 60 dB in Scenario V (shown in figures 5(c) and (d)), the singular energy component becomes noisier but its singular peak can still be identified by increasing the DWT level to 5. However, when the noise level increases to SNR 50 dB in Scenario VI (shown in figures 5(e) and (f)), the singular peak becomes ambiguous because of other fake peaks caused by the noise, even at a higher DWT level of 6. Thus, SNR 60 dB can be regarded as the noise tolerance of the proposed method in this numerical case.

With such limit SNR, the singular peak becomes less pronounced to evidently indicate any damage when the delamination size decreases. Thus, the minimum delamination size could be detected by the proposed method is 20 mm × 20 mm in this numerical case.
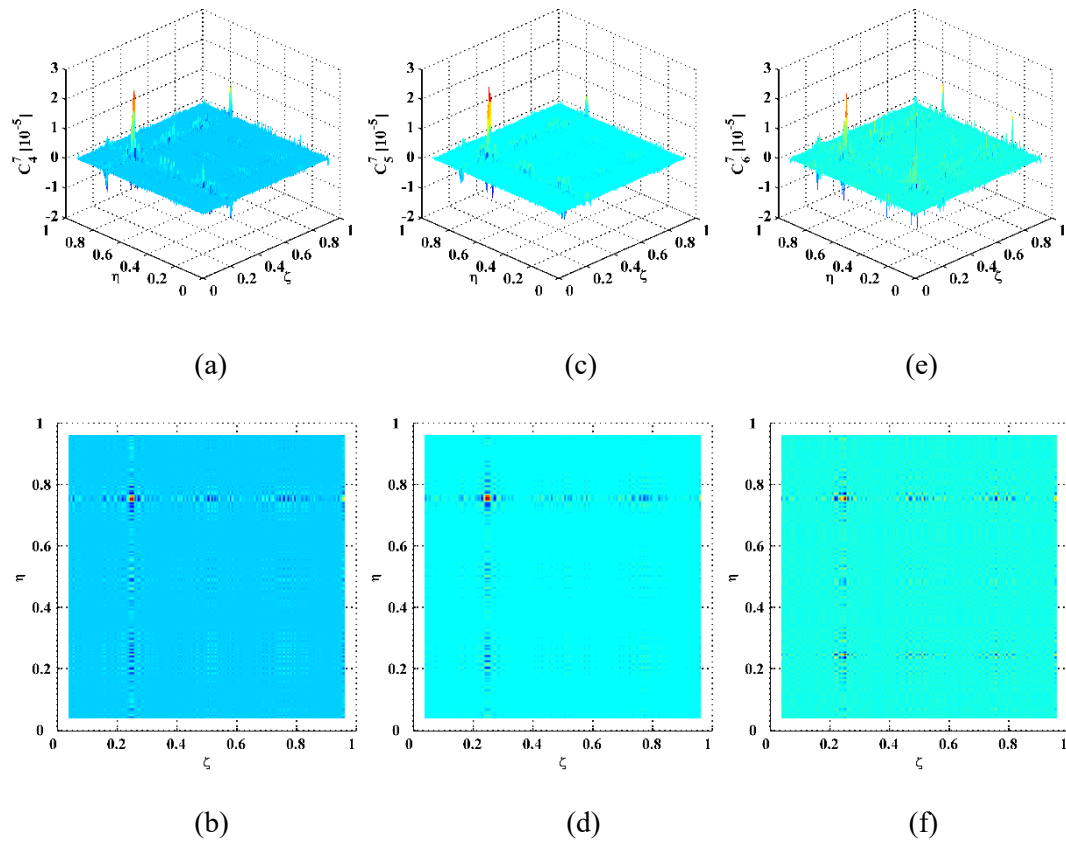
Figure 5. Singular energy components for Scenarios (a) IV, (c) V, and (e) VI, and their planforms (b) IV, (d) V, and (f) VI.

It is worth noting that the computational efficiency of the proposed method is mainly determined by the DWT in equation (8). Higher DWT level requires more computing time: it takes 10.4, 13.1, and 15.8 s to do the DWT in Scenarios IV, V, and VI with respective levels of 4, 5, and 6. On the other hand, for all numerical scenarios, total computation time of 0.1 s is almost the same to do the computation in equations (9) to (11). The computation was done in Matlab using an ordinary desktop computer

4. Experimental validation

4.1. Experimental set-up

The applicability of the singular energy component for identifying initial delamination is experimentally validated on an eight-ply CFRP (GG204P IMP503 42) symmetric cross-ply laminate made of 0/90° orientations. The dimensions of the CFRP laminate are 500 mm × 500 mm × 3 mm in the x-, y-, and z-directions, respectively. To manufacture an initial delamination, a square Teflon sheet (15 mm × 15 mm) was inserted between the interfaces of the second and third plies when the CFRP laminate was fabricated. The delamination is centered at x=125 mm and y=375 mm, spanning from 117.5 mm to 132.5 mm and 367.5 mm to 382.5 mm in the x- and y-directions, respectively. In the dimensionless coordinates, the delamination is centered at $\zeta = 0.25$ and $\eta = 0.75$, spanning from 0.235 to 0.265 and 0.735 to 0.765 in the $\zeta -$ and $\eta -$ directions, respectively. The experimental specimen and set-up are shown in figure 6. The CFRP laminate is suspended by two strings in its two upper corners, to simulate free boundary conditions for simplicity and repeatability of experiments [46]. It is worth mentioning that the proposed method can be applied to laminates with other boundary conditions, because the concept of MRM-TKE^{2D} is independent of boundary conditions [37]. The surfaces of the CFRP laminate are entirely flat and the delamination is barely visible from the appearance, even in the zoomed-in view in figure 6. Outlines of the delamination location are marked in white on the front surface (the surface of the laminate that belongs to the first ply is defined as the front surface and the other surface is the back surface). At the geometrical center of the front surface, a circular PZT piezoelectric actuator with the diameter of 10 mm is placed to generate high-frequency

harmonic wave to excite the CFRP laminate. Synchronously, a SLV (Polytec PSV-400) is employed to scan the entire back surface covered by reflection tapes with 375×375 densely-distributed measurement points whose interval is about 1.33 mm. For clearer illustration, a schematic of the enhanced PZT-SLV system for initial delamination identification in the CFRP laminate is illustrated in figure 7. The enhanced PZT-SLV system with high frequency and high resolution can facilitate identification of initial delamination.
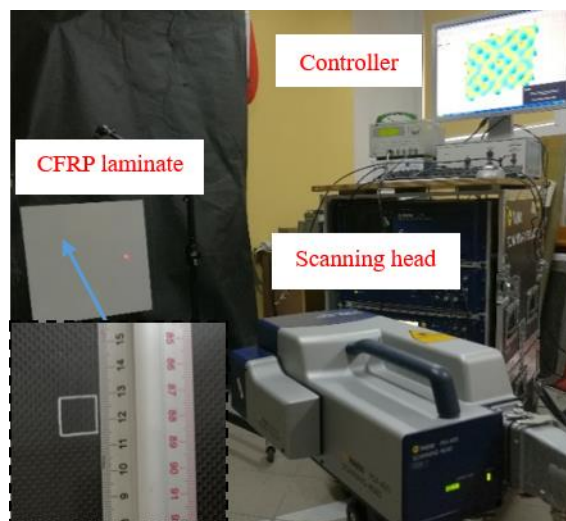
Figure 6. Experimental specimen and set-up: delaminated CFRP laminate and enhanced PZT-SLV system.
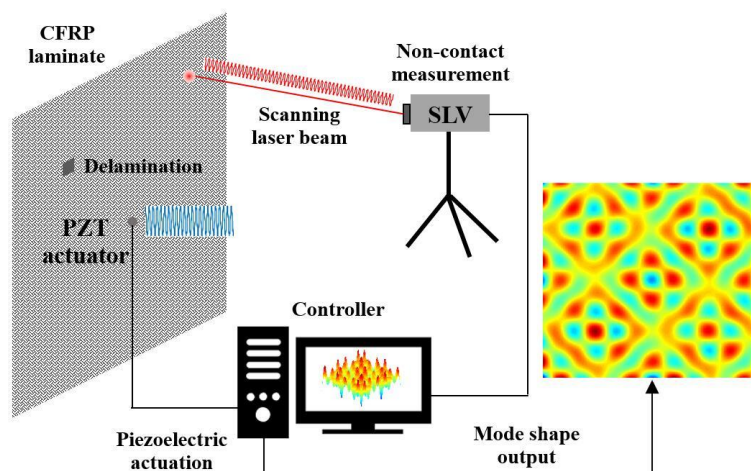
Figure 7. Schematic of enhanced PZT-SLV system for delamination identification in CFRP

laminate.

4.2. Experimental results

After modal analysis over a broad frequency range [47], mode shapes can be acquired by the SLV. A high-order mode shape at 5309.37 Hz is selected and shown in figure 8(a) with a unit maximum amplitude. The MRM-TKE^{2D} at the sixth level E_6 for the measured mode shape is obtained by equations (8) and (9), shown in figure 8(b), where no evident feature appears to indicate any delamination feature. To find the singular energy component, E_6 is decomposed into components by equations (10) and (11), whose spectral entropies are calculated by equations (12) to (14) and shown in figure 9. It can be seen from figure 9 that the global trend status, the transient state, and the noise status are divided by two grey dashed lines. The singular energy component can be searched from the 11th to the 23rd energy components.

(a)   (b)
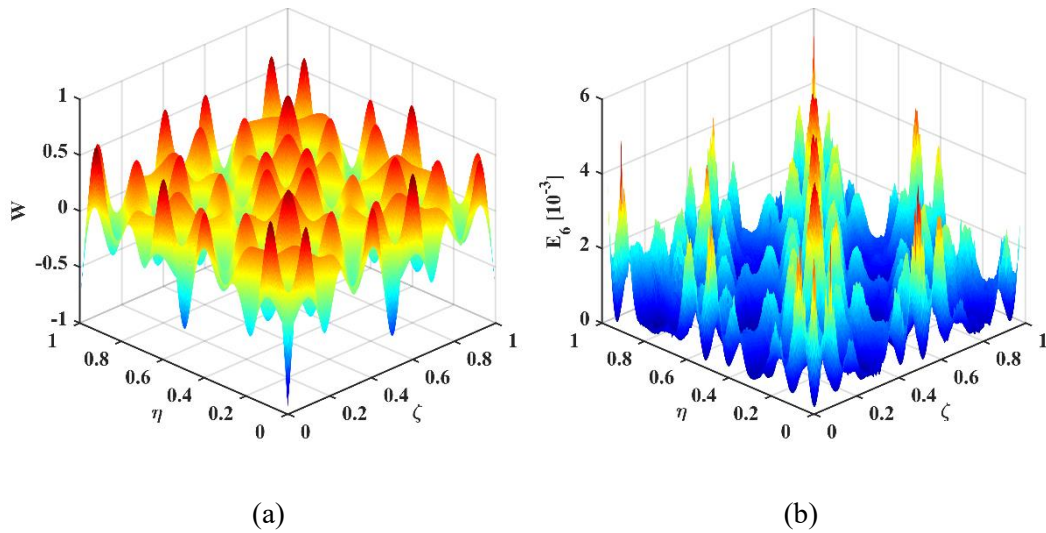
Figure 8. (a) Measured mode shape and its (b) MRM-TKE^{2D}.
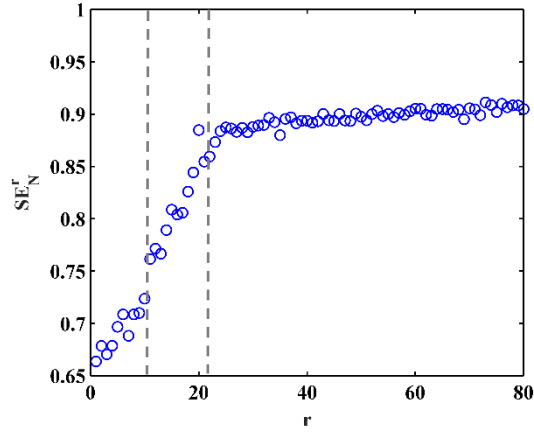
Figure 9. Spectral entropies of MRM-TKE[2D] components.

Among these energy components (figure 10), the first five energy components constitute the global trend of the MRM-TKE[2D] (weights of C_6^1, C_6^2, and C_6^3 are 37.81% 18.22%, and 6.63%, respectively). The 11th energy component that converges into the delamination region is determined as the singular energy component (figure 11(a)). In its planform (figure 11(b)), the singular peak clearly shows that the delamination is centered at $\zeta = 0.25$ and $\eta = 0.75$, spanning from about 0.235 to 0.265 and 0.735 to 0.765 in the $\zeta-$ and $\eta-$ directions, respectively, in good agreement with the actual location and size of the initial delamination.
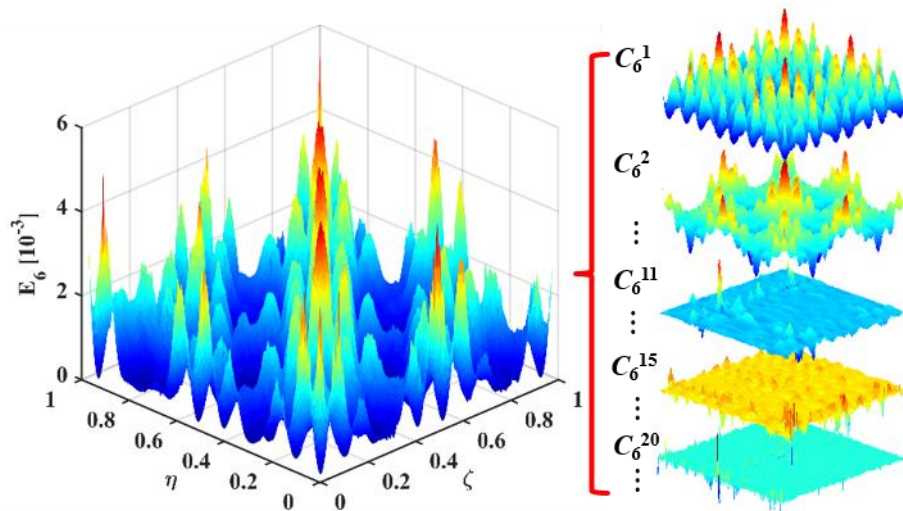
Figure 10. MRM-TKE^{2D} and its components.

(a)   (b)
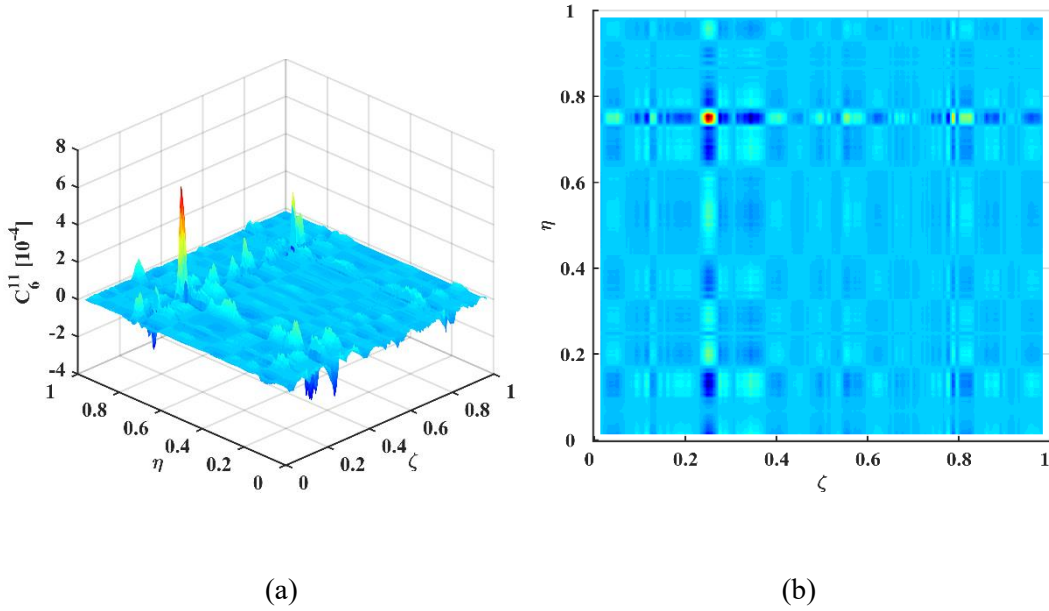
Figure 11. Singular energy component in (a) MRM-TKE^{2D} and (b) its planform.

To explore the effectiveness of the proposed method for different excitation locations and frequencies, excitation at another natural frequency of 3504.68 Hz is applied to the lower right corner of the laminate. Corresponding mode shape is shown in figure 12(a) with a unit maximum amplitude, whose MRM-TKE^{2D} at the sixth DWT level E_6 shape is obtained by equations (3) and (4), shown in figure 12(b). The 11th energy component is found by the spectral entropies, in which energy converges into the delamination region to form a sharply rising singular peak and almost vanishes in other places (figure 13(a)). Thus, the presence of the delamination can be well detected. In its planform (figure 13(b)), the location and size of the delamination is well characterized to be centered at $\zeta = 0.25$ and $\eta = 0.75$, spanning from about 0.235 to

0.265 and 0.735 to 0.765 in the $\zeta-$ and $\eta-$ directions, respectively. The location and

size of the delamination identified in figure 13 corresponds well with that in figure 11,

substantiating that the proposed method is adaptive to different excitation locations and

frequencies. Worth to be mentioned, it takes 13.7 s to do the DWT in equation (8) and

0.1 s to do the computation in equations (9) to (11).

(a)   (b)
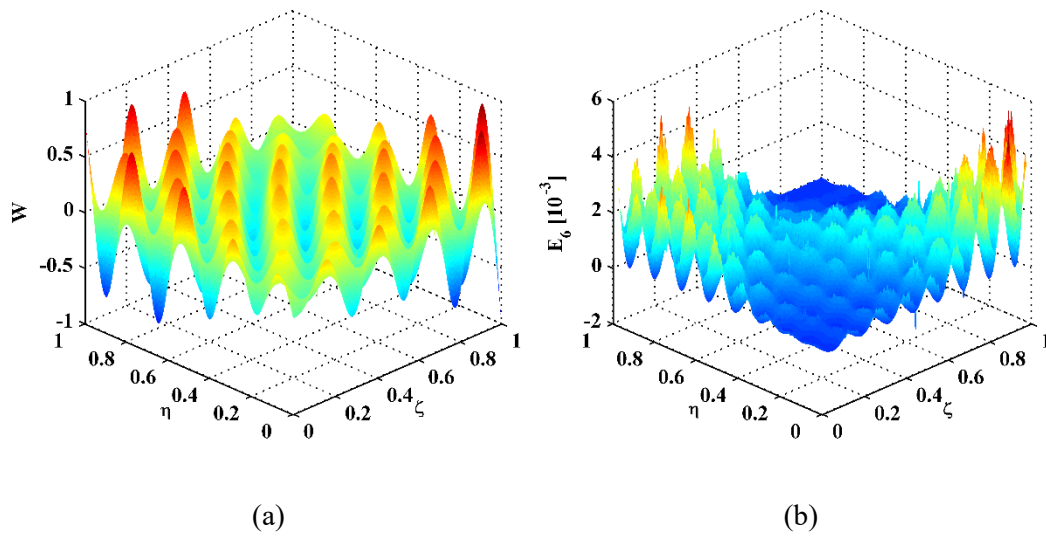
Figure 12. (a) Measured mode shape and its (b) MRM-TKE^{2D}.

(a)   (b)
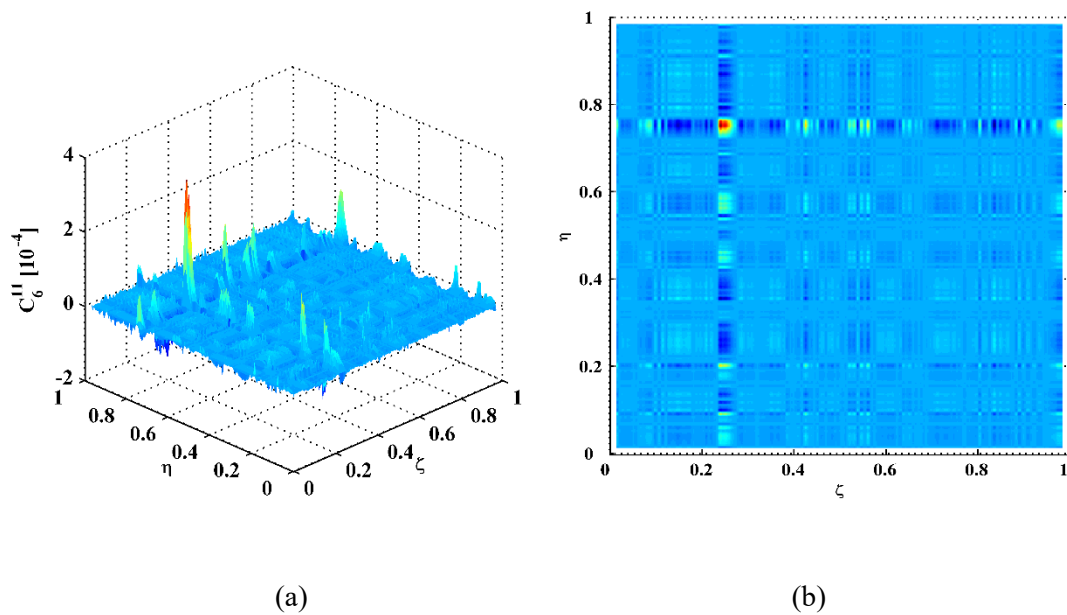
Figure 13. (a) Singular energy component in MRM-TKE^{2D} and (b) its planform.

For the specimen of CFRP laminate used in this study, the minimum delamination size can be detected by the method is 15 mm × 15 mm at the actual noise level during the measurement in the laboratory. For identification of smaller delamination, the delamination-caused singular peak will probably become less pronounced; besides, denser spatial sampling of laser scanning will be time consuming.

Worth to be mentioned, for real-word structural components including composite laminates, damage identification methods relying on laser scanning will encounter some difficulties, such as costs and agility to carry a SLV for industrial applications, identification of damage in structures in use, accessibility to structural components that are not easy to inspect. With these concerns, Park et al. [48] have discussed the applicability of laser scanning to delamination detection in wind turbine blades. As the SLV has long-range inspection up to 10s of meters, it can be carried on a vehicle to inspect real structural components. For structures in use, inspected components need to suspend operation for inspection, which requires fast scanning strategy to reduce scanning time. For structural components in locations that are not easy to directly inspect, laser beams scanning on surfaces of inspected components could be reflected from the SLV by mirrors.

5. Concluding remarks

It is difficult to identify initial delamination in the early stage, which is typically BVID in composite laminates. Recently, the concept of the MRM-TKE^{2D} was proposed to reveal delamination-caused singularity in a mode shape for delamination identification

with high robustness against environmental noise. Addressing the inadequate sensitivity of the MRM-TKE^{2D} to initial delamination, a scheme of decomposing the MRM-TKE^{2D} into components is proposed in this study to resolve this problem. The singular energy component among the energy components can be found for identification of initial delamination. The capability of the proposed method is validated by numerical and experimental results. Some concluding remarks follow.

(1) For spectral entropies of energy components of the MRM-TKE^{2D}, its singular energy component appears in the transient status, in which the values of the spectral entropies increase rapidly because more uncertain information is introduced and distributed in a wider frequency band.

(2) In the singular energy component that is dominated by the delamination, energy converges into the delamination region to form a singular peak and almost vanishes in other places, whereby the presence and location of the initial delamination can be characterized.

(3) For initial delamination identification, high-frequency harmonic waves at kilohertz are generated by a PZT piezoelectric actuator to excite the laminate, whereby high-order modes can be achieved. Synchronously, corresponding high-order mode shapes are measured at millimeter-level high resolution by a non-contact SLV to capture details of the initial delamination. Thereby, the enhanced PZT-SLV system with high frequency and high resolution facilitates the identification of initial delamination.

References:

[1]   Katunin A, Dragan K and Dziendzikowski M 2015 Damage identification in aircraft composite structures: A case study using various non-destructive testing techniques *Composite Structures* 127 1-9

[2]   Manoach E, Warminski J, Mitura A and Samborski S 2012 Dynamics of a composite Timoshenko beam with delamination *Mechanics Research Communications* 46 47-53

[3]   Cantwell W J and Morton J 1985 Detection of impact damage in CFRP laminates *Composite Structures* 3 241-257

[4]   Komorowski J P, Simspson D L and Gould R W 1990 A technique for rapid impact damage detection with implication for composite aircraft structures *Composites* 21 169-173

[5]   Hosur M V, Murthy C, Ramamurthy T S and Shet A 1998 Estimation of impact-induced damage in CFRP laminates through ultrasonic imaging *NDT and E International* 31 359-374

[6]   Tsutsui H, Kawamata A, Kimoto J, Isoe A, Hirose Y, Sanda T and Takeda N 2004 Impact damage detection system using small-diameter optical-fiber sensors embedded in CFRP laminate structures *Advanced Composite Materials* 13 43-55

[7]   Tsutsui H, Kawamata A, Sanda T and Takeda N 2004 Detection of impact damage of stiffened composite panels using embedded small-diameter optical fibers *Smart Materials and Structures* 13 1284-1290

[8]   Takeda S, Minakuchi S, Okabe Y and Takeda N 2005 Delamination monitoring

of laminated composites subjected to low-velocity impact using small-diameter FBG sensors *Composites Part A-Applied Science and Manufacturing* 36 903-908

[9] Frieden J, Cugnoni J, Botsis J and Gmuer T 2012 Low energy impact damage monitoring of composites using dynamic strain signals from FBG sensors - Part I: Impact detection and localization *Composite Structures* 94 438-445

[10] Frieden J, Cugnoni J, Botsis J and Gmuer T 2012 Low energy impact damage monitoring of composites using dynamic strain signals from FBG sensors - Part II: Damage identification *Composite Structures* 94 593-600

[11] Graham D, Maas P, Donaldson G B and Carr C 2004 Impact damage detection in carbon fibre composites using HTS SQUIDs and neural networks *NDT and E International* 37 565-570

[12] Liang T, Ren W, Tian G Y, Elradi M and Gao Y 2016 Low energy impact damage detection in CFRP using eddy current pulsed thermography *Composite Structures* 143 352-361

[13] Angelidis N and Irving P E 2007 Detection of impact damage in CFRP laminates by means of electrical potential techniques *Composites Science and Technology* 67 594-604

[14] Ball R J and Almond D P 1998 The detection and measurement of impact damage in thick carbon fibre reinforced laminates by transient thermography *NDT and E International* 31 165-173

[15] Barden T J, Almond D P, Pickering S G, Morbidini M and Cawley P 2007 Detection of impact damage in CFRP composites by thermosonics *Nondestructive*

Testing and Evaluation 22 71-82

[16] Pieczonka L, Aymerich F, Brozek G, Szwedo M, Staszewski W J and Uhl T 2013 Modelling and numerical simulations of vibrothermography for impact damage detection in composites structures *Structural Control and Health Monitoring* 20 626-638

[17] Maier A, Schmidt R, Oswald-Tranta B and Schledjewski R 2014 Non-destructive thermography analysis of impact damage on large-scale CFRP automotive parts *Materials* 7 413-429

[18] Gryzagoridis J and Findeis D 2010 Impact damage detection on composites using optical NDT techniques *Insight* 52 248-251

[19] Su Z, Ye L and Lu Y 2006 Guided Lamb waves for identification of damage in composite structures: A review *Journal of Sound and Vibration* 295 753-780

[20] Eremin A, Golub M, Glushkov E and Glushkova N 2019 Identification of delamination based on the Lamb wave scattering resonance frequencies *NDT and E International* 103 145–153

[21] Su Z, Yang C, Pan N, Ye L and Zhou L 2007 Assessment of delamination in composite beams using shear horizontal (SH) wave mode *Composite Science and Technology* 67 244-251

[22] Quaegebeur N, Micheau P, Masson P and Maslouhi A 2010 Structural health monitoring strategy for detection of interlaminar delamination in composite plates *Smart Materials and Structures* 19 085005

[23] Hettler J, Tabatabaeipour M, Delrue S and Van Den Abeele K 2016 Linear and

nonlinear guided wave imaging of impact damage in CFRP using a probabilistic approach *Materials* 9 901

[24] Solodov I and Busse G 2007 Nonlinear air-coupled emission: The signature to reveal and image microdamage in solid materials *Applied Physics Letters* 91 251910

[25] Polimeno U and Meo M 2009 Detecting barely visible impact damage detection on aircraft composites structures *Composite Structures* 91 398-402

[26] Aymerich F and Staszewski W J 2010 Impact damage detection in composite laminates using nonlinear acoustics *Composites Part A: Applied Science and Manufacturing* 41 1084-1092

[27] Klepka A, Staszewski W J, di Maio D and Scarpa F 2013 Impact damage detection in composite chiral sandwich panels using nonlinear vibro-acoustic modulations *Smart Materials and Structures* 22 084011

[28] Pieczonka L, Ukowski P, Klepka A, Staszewski W J, Uhl T and Aymerich F 2014 Impact damage detection in light composite sandwich panels using piezo-based nonlinear vibro-acoustic modulations *Smart Materials and Structures* 23 105021

[29] Fan W and Qiao P 2011 Vibration-based damage identification methods: A review and comparative study *Structural Health Monitoring-An International Journal* 10 83-111

[30] Qiao P, Lu K, Lestari W and Wang J 2007 Curvature mode shape-based damage detection in composite laminated plates *Composite Structures* 80 409-428

[31] Araújo dos Santos J V, Lopes H M R, Vaz M, Soares C M M, Soares C A M and

De Freitas M J M 2006 Damage localization in laminated composite plates using mode shapes measured by pulsed TV holography *Composite Structures* 76 272-281

[32] Pérez M A, Gil L and Oller S 2014 Impact damage identification in composite laminates using vibration testing *Composite Structures* 108 267-276

[33] Cao M S, Ostachowicz W, Radzieński M and Xu W 2013 Multiscale shear-strain gradient for detecting delamination in composite laminates *Applied Physics Letters* 103 101910

[34] Xu W, Cao M S, Li X M, Radzieński M, Ostachowicz W and Bai R B 2017 Delamination monitoring in CFRP laminated plates under noisy conditions using complex-wavelet 2D curvature mode shapes *Smart Material and Structures* 26 104008

[35] Chen D M, Xu Y F and Zhu W D 2018 Non-model-based identification of delamination in laminated composite plates using a continuously scanning laser Doppler vibrometer system *Journal of Vibration and Acoustics* 140(4) 041001

[36] Solodov I, Bai J, Bekgulyan S and Busse G 2011 A local defect resonance to enhance acoustic wave-defect interaction in ultrasonic nondestructive evaluation *Applied Physics Letters* 99 211911

[37] Xu W, Fang H, Cao M, Zhou L, Wang Q and Ostachowicz W 2019 A noise-robust damage indicator for characterizing singularity of mode shapes for incipient delamination identification in CFRP laminates *Mechanical Systems and Signal Processing* 121 183-200

[38] Leissa A W and Qatu M S 2011 Vibration of continuous systems *McGraw Hill*

[39] Zhao Y, Noori M, Altabey W, Ghiasi R and Wu Z 2019 A fatigue damage model for FRP composite laminate systems based on stiffness reduction *Structural Durability & Health Monitoring* 13 85-103

[40] Cao M, Radzieński M, Ostachowicz W and Xu W 2013 Multiscale characterization of damage in plates based on 2D Mexican wavelet *Health Monitoring of Structural and Biological Systems 2013* 8695 pp 869537

[41] Mallat S 2008 A Wavelet Tour of Signal Processing *Academic Press San Diego*

[42] Kaiser J F 1990 On a simple algorithm to calculate the 'energy' of a signal *International Conference on Acoustics, Speech, and Signal Processing* pp 381-384

[43] Boudraa A and Diop E S 2008 Image contrast enhancement based on 2D Teager-Kaiser operator *IEEE International Conference on Image Processing* pp 3180-3183

[44] Stewart G W 1993 On the early history of the singular value decomposition *SIAM Review* 35 551-566

[45] Pan Y N, Chen J and Li X L 2009 Spectral entropy: a complementary index for rolling element bearing performance degradation assessment *2009 Proceedings of the Institution of Mechanical Engineers, Part C: Journal of Mechanical Engineering Science* 223(5) 1223-1231

[46] Yoon M K, Heider D, Gillespie J W, Ratcliffe C P and Crane R M 2005 Local damage detection using the two-dimensional gapped smoothing method *Journal*

of Sound and Vibration 279(1–2) 119–139.

[47] Xu H, Zeng Z, Wu Z, Zhou L, Su Z, Liao Y and Liu M 2017 Broadband dynamic responses of flexible carbon black/poly (vinylidene fluoride) nanocomposites: A sensitivity study *Composite Science and Technology* 149 246-253

[48] Park B, Sohn H, Malinowski P and Ostachowicz W 2017 Delamination localization in wind turbine blades based on adaptive time-of-flight analysis of noncontact laser ultrasonic signals *Nondestructive Testing and Evaluation* 32 1-20